VIP Catalysis Very Important Paper

How to cite: *Angew. Chem. Int. Ed.* **2020**, *59*, 19592–19601
International Edition: doi.org/10.1002/anie.202007147
German Edition: doi.org/10.1002/ange.202007147

Ethylene Dehydroaromatization over Ga-ZSM-5 Catalysts: Nature and Role of Gallium Speciation

Yunwen Zhou, Hari Thirumalai, Scott K. Smith, Kenton H. Whitmire, Jing Liu, Anatoly I. Frenkel, Lars C. Grabow, and Jeffrey D. Rimer**

Abstract: *Bifunctional catalysis in zeolites possessing both Brønsted and Lewis acid sites offers unique opportunities to tailor shape selectivity and enhance catalyst performance. Here, we examine the impact of framework and extra-framework gallium species on enriched aromatics production in zeolite ZSM-5. We compare three distinct methods of preparing Ga-ZSM-5 and reveal direct (single step) synthesis leads to optimal catalysts compared to post-synthesis methods. Using a combination of state-of-the-art characterization, catalyst testing, and density functional theory calculations, we show that Ga Lewis acid sites strongly favor aromatization. Our findings also suggest Ga(framework)–Ga(extra-framework) pairings, which can only be achieved in materials prepared by direct synthesis, are the most energetically favorable sites for reaction pathways leading to aromatics. Calculated acid site exchange energies between extra-framework Ga at framework sites comprised of either Al or Ga reveal a site-specific preference for stabilizing Lewis acids, which is qualitatively consistent with experimental measurements. These findings indicate the possibility of tailoring Lewis acid siting by the placement of Ga heteroatoms at distinct tetrahedral sites in the zeolite framework, which can have a marked impact on catalyst performance relative to conventional H-ZSM-5.*

Introduction

Benzene, toluene, and xylene (BTX) are important precursors in the petrochemical industry for the production of polymers, fuel additives, and other value-added products.[1] Zeolite ZSM-5 (MFI type) has been demonstrated to be a superb catalyst for BTX production from different feedstocks, including syngas,[2] methanol,[3] light alkanes[4] and alkenes,[5] due to its unique medium pore (10-member ring) shape selectivity. Modified Brønsted acidic H-ZSM-5 catalysts with metals (e.g. Ag, Ga, Zn) forming Lewis acid sites have demonstrated exceptional enhanced aromatics yield for non-oxidative dehydroaromatization (DHA) of ethylene and propylene.[5b,c,6] Moreover, Ga-ZSM-5 has been used in dehydrogenation reactions,[7] including the commercial UOP/BP Cyclar process to convert light alkanes to aromatics.[8] Despite numerous studies of Ga-zeolites, a general understanding of active sites and the potential synergy between Lewis and Brønsted acids is lacking.

In addition to Ga-ZSM-5, prior studies have also characterized structure-performance relationships for Ga-exchanged chabazite (CHA) and beta (*BEA) catalysts.[9] There are two conventional post-synthetic approaches to prepare Ga-modified zeolites: (1) solution ion exchange with a gallium salt (e.g. $Ga(NO_3)_3$); and (2) incipient-wetness impregnation.[7a] Characterization of Ga-zeolites prepared by these methods often reveals large fractions of Ga_xO_y deposits on external surfaces of zeolite particles owing to the slow diffusion of hydrated Ga ionic species into the nanopores.[10] To obtain more dispersed Ga species within zeolite pores, it has been shown that Ga_xO_y can be reduced under H_2 at high temperature (>700 K) to facilitate Ga migration into pores and ion exchange with Brønsted acid sites.[11] Price et al. investigated the effects of various treatment methods on the state of Ga (in ZSM-5 catalysts) and the aromatization activity in DHA reactions.[11b,12] They observed that the optimal catalyst was prepared by reduction of Ga_xO_y to dispersed Ga species and reoxidation to obtain Ga^{3+} sites within the 3-dimensional pores of ZSM-5; however, it has been hypothesized that achieving a uniform dispersion of Ga^{3+} sites by this method is challenging.[10] Bell and coworkers prepared isolated Ga^{3+} cations inside H-ZSM-5 using

[*] Dr. Y. Zhou, Dr. H. Thirumalai, Prof. L. C. Grabow, Prof. J. D. Rimer
Department of Chemical and Biomolecular Engineering,
University of Houston
Houston, TX 77204 (USA)
E-mail: grabow@uh.edu
jrimer@central.uh.edu
Dr. S. K. Smith, Prof. L. C. Grabow, Prof. J. D. Rimer
Department of Chemistry, University of Houston
Houston, TX 77204 (USA)
Prof. K. H. Whitmire
Department of Chemistry, Rice University
Houston, TX 77005 (USA)
Prof. J. Liu
Physics Department, Manhattan College
Riverdale, NY 10471 (USA)
Prof. A. I. Frenkel
Department of Materials Science and Chemical Engineering,
Stony Brook University
Stony Brook, NY 11794 (USA)
and
Chemistry Division, Brookhaven National Laboratory
Upton, NY 11973 (USA)
Prof. L. C. Grabow
Texas Center for Superconductivity at the University of Houston (TcSUH), University of Houston
Houston, TX 77204 (USA)
Supporting information and the ORCID identification number(s) for the author(s) of this article can be found under:
https://doi.org/10.1002/anie.202007147.

vapor-phase exchange with $GaCl_3$,[7d,11a] and investigated the mechanism and kinetics of propane dehydrogenation over Ga-ZSM-5 catalysts. They report $[GaH]^{2+}$ is the active site for both propane dehydrogenation and cracking reactions.[7d] Lercher and co-workers used conventional wetness impregnation to prepare well-characterized Ga-ZSM-5 catalysts for propane dehydrogenation wherein they reported Lewis-Brønsted acid pairs are essential to catalyze the reaction.[13] They proposed the existence of Ga^+ sites that can be protonated by proximal Brønsted acids to form $[GaH]^{2+}$. Bell and Lercher both claim $[GaH]^{2+}$ is the active species for propane dehydrogenation, though there are differences in their proposed reaction mechanisms. This active site, however, is more probable for zeolites with low Si/Al ratio as it requires two anionic framework Al sites in close proximity.

Ga-ZSM-5 catalysts prepared via direct synthesis have been shown to enhance aromatics selectivity in alkane dehydrogenation reactions.[11c,14] Jones and co-workers[7b] developed a method using synthesis mixtures with 3-mercaptopropyl-trimethoxysilane (MPS) to generate gallosilicates with a high percentage of Ga Lewis acid sites occluded as extra-framework species into zeolite pores without directly forming covalent bonds with framework oxygens. The resulting gallosilicate catalyst (i.e. Ga-MFI in the absence of Al) enhanced rates of propane dehydrogenation compared to gallosilicates prepared by conventional methods. Shu and co-workers evaluated several Ga-ZSM-5 catalysts obtained via different methods (i.e. direct synthesis, ion exchange, impregnation, and physical mixing) on n-heptane aromatization.[15] They reported the Ga-ZSM-5 catalyst prepared by direct synthesis exhibited the highest BTX selectivity, which they attribute to enhanced Lewis acidity and the presumed mesoporosity incurred by the incorporation of framework Ga. Moreover, they hypothesized that both liquid-phase ion exchange and direct synthesis lead to Ga substitution in framework sites. On the contrary, Hsieh et al.[16] argued that Ga is less prone to be incorporated into the zeolite framework (compared to Al) based on their analysis of [Ga, Al]-ZSM-5 catalysts obtained via seeded synthesis.

Ga species supported on microporous materials can be difficult to characterize due to the complexity of zeolite topology and interactions with strong Brønsted acid sites. To this end, Scott and co-workers systematically examined nonporous catalysts (e.g. $Ga(i\text{-}Bu)_3$ grafted onto γ-alumina and silica) for propane dehydrogenation wherein they showed that mononuclear alumina-supported Ga sites exhibit higher activity than silica-supported Ga sites;[17] and using a combination of high-field solid-state nuclear magnetic resonance (NMR) spectroscopy and X-ray absorption spectroscopy (XAS), they showed that each Ga species has a tetrahedral coordination and resolved their location on oxide supports. For Ga-zeolites, the number of potential Ga species reported in literature (Scheme 1) includes the following: Ga_xO_y, Ga^+, $[GaO]^+$, $[GaH_2]^+$, $[Ga(OH)_2]^+$, $[GaH(OH)]^+$, and $[GaH]^{2+}$.[7d,11b,18] With the exception of Ga^+ these species contain Ga in its +3 oxidation state. For direct synthesis, Ga incorporated in framework sites (Scheme 1 A) may also lead to the generation of Brønsted acid sites.[19]

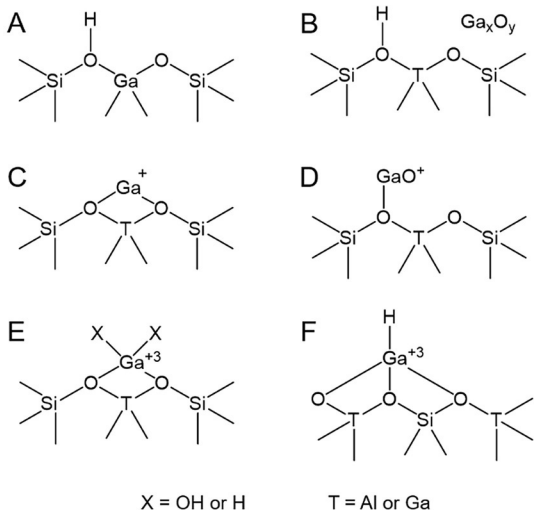

Scheme 1. Possible zeolite Brønsted and Lewis acid sites generated from heteroatom framework (T = Al or Ga) and/or extra-framework species: A) framework Ga^{3+}; B) Ga_xO_y; C) Ga^+; D) $[GaO]^+$; E) $[GaH_2]^+$, $[Ga(OH)_2]^+$, or $[GaH(OH)]^+$; and F) $[GaH]^{2+}$.

Herein, we investigate the speciation and siting of Ga in ZSM-5 catalysts, and correlate the synergy of Brønsted and Lewis acid sites on the ethylene DHA reaction. We systematically examine five Ga-ZSM-5 zeolite catalysts prepared via different treatments, including both direct synthesis and post-synthesis exchange. Using a combination of experimental techniques, including XAS and solid-state ^{27}Al and ^{71}Ga magic angle spinning (MAS) NMR spectroscopy, we distinguish Ga species with different oxidation states and coordination numbers. The catalytic performance of various Ga-ZSM-5 catalysts helps differentiate the roles of (extra-) framework Ga species. Experimental characterization and catalytic studies were coupled with density functional theory (DFT) calculations to assess the relative activities of different Ga and Al sites. Collectively, these findings highlight the challenges of elucidating Ga speciation, and the impact of Ga-ZSM-5 preparation on enhanced activity for the promotion of aromatics (i.e. BTX products).

Results and Discussion

Ga-ZSM-5 catalysts were prepared by three distinct methods of gallium occlusion. The first method is a direct synthesis adapted from a previous study[7b] that places Ga in either extra-framework (EFW) or framework (FW) sites. Inductively coupled plasma analysis in combination with optical emission spectroscopy (ICP-OES) reveals the product of direct synthesis contains a molar composition of Si:Al:Ga = 57:2.4:1.0. This sample is referred to herein as Ga-Z1. The second and third methods involved post-synthesis modifications to a commercial ZSM-5 (Zeolyst CBV 5524G, referred to as Z-ref) with nearly identical molar Si/Al ratio as that of Ga-Z1 (Table 1). In one approach we used solution ion exchange with $Ga(NO_3)_3$ to produce a product, referred to as Ga-Z2. In the second approach we used vapor-phase ex-

Table 1: Elemental analysis of H-zeolite catalyst samples.

Sample[d]	Sample Preparation	Composition[a]		Al content [%][b]	
		Si/Al	Si/Ga	Al_{FW}	Al_{EFW}
Ga-Z1	Direct synthesis	24	57	89	11
Ga-Z2	Solution ion exchange	30	54	94	6
Ga-Z3	Vapor phase exchange	30	54	85	15
Ga-Z1H	Z1 with H_2 treatment	24	57	91	9
Ga-Z2H	Z2 with H_2 treatment	31	54	94	6
Z-ref	Commercial zeolite	29[c]	–	94	6

[a] Determined by ICP-OES; [b] Measured by ^{27}Al MAS NMR spectra of hydrated zeolite materials (Figure S1); [c] Value of commercial zeolite CBV 5524G (Zeolyst) reported by Phadke et al.;[11a] [d] SEM images of samples reveal a spheroidal morphology with average particle sizes in the range of 300–500 nm (Figure S2).

change with $GaCl_3$ according to a protocol reported by Bell and co-workers[11a] (referred to as sample Ga-Z3). The molar compositions of samples Ga-Z2 and Ga-Z3 are both equal to Si:Al:Ga = 54:1.8:1.0.

The solution ion exchange method reportedly leads to a large fraction of Ga_xO_y species deposited on the external surfaces of ZSM-5.[10,20] Using a previous approach[18a] to obtain more dispersed Ga species, samples Ga-Z1 and Ga-Z2 were treated in H_2 at 848 K and are referred to herein as Ga-Z1H and Ga-Z2H, respectively (note that the protocol for Ga-Z3 also involves H_2 treatment at 823 K). The aluminum speciation for each sample was quantified using solid-state NMR (Figure S1) where peaks at 55 ppm and 0 ppm in ^{27}Al MAS NMR spectra correspond to tetrahedral Al_{FW} (framework Al) and octahedral Al_{EFW} (extra-framework Al), respectively.[21] The percentages of Al species for each sample are listed in Table 1, showing that Al speciation is not altered by either solution ion exchange or H_2 treatment; however, there is a 9% reduction in Al_{FW} (with concomitant increase in Al_{EFW}) during Ga impregnation by chemical vapor-phase exchange, as observed for Ga-Z3 (compared to the parent Z-ref). This is likely due to the release of HCl during the decomposition of $GaCl_3$, which could facilitate dealumination of the zeolite framework.

Powder X-ray diffraction (PXRD) patterns confirmed the structural integrity (MFI framework) of all calcined H-Ga-ZSM-5 catalysts (Figure S3) and the absence of impurities in Ga-Z1. It has been reported[10] that solution ion exchange can lead to the formation of crystalline Ga_xO_y that is not visible in the PXRD pattern of Ga-Z2; however, samples prepared by ion exchange with higher Ga concentrations (Table S1) clearly show the presence of crystalline Ga_xO_y by PXRD (i.e. peaks at $2\theta = 21.6°$ and 37.1° in Figure S4).[22] It has also been reported[16] that PXRD patterns can provide evidence of Ga incorporation in framework sites based on shifts in two characteristic MFI peaks, (501) and (303), when a larger Ga atom replaces a smaller Al atom. For all H-Ga-ZSM-5 samples in this study, these two peaks (at $2\theta = 23.0°$ and 23.8°, respectively) exhibit no observable shifts compared to commercial zeolite, Z-ref (Figure S3). This seems to suggest the majority of Ga may be present as extra-framework species.

X-ray absorption fine structure (XAFS) spectroscopy was used to characterize the changes in the local structure and electronic state of Ga between samples Ga-Z1 and Ga-Z2 (a similar analysis of Ga-Z3 has been reported by Phadke et al.[11a] and is repeated in the Supporting Information). X-ray absorption near edge structure (XANES) data at the Ga K-edge (Figure 1A) show that the absorption edge energy is very similar between Ga-Z1 and Ga-Z2, while the main peak region is broadened for Ga-Z2. The absorption edge energy is defined here as the first inflection point of the XANES spectrum and is related to the charge state of the probed atoms. The charge state of Ga atoms in both samples is, effectively, +3 since the position of the absorption edge energy is at ca. 10376 eV for both samples, similar to the value of the reported standard Ga^{3+} species.[11a] The variation between XANES features in these two H-Ga-ZSM-5 samples is evidence of differences in their local environments.

Fourier transform magnitude of the k^2-weighted extended X-ray absorption fine structure (EXAFS) spectrum (Figure 1B) of Ga-Z2 features a shoulder near the 2 Å distance that is absent for the Ga-Z1 sample. Moreover, the first peak between 1 and 2 Å in the spectrum of Ga-Z2 is slightly shifted to higher distance compared to that of Ga-Z1. These observations, together with the large signal in the region of

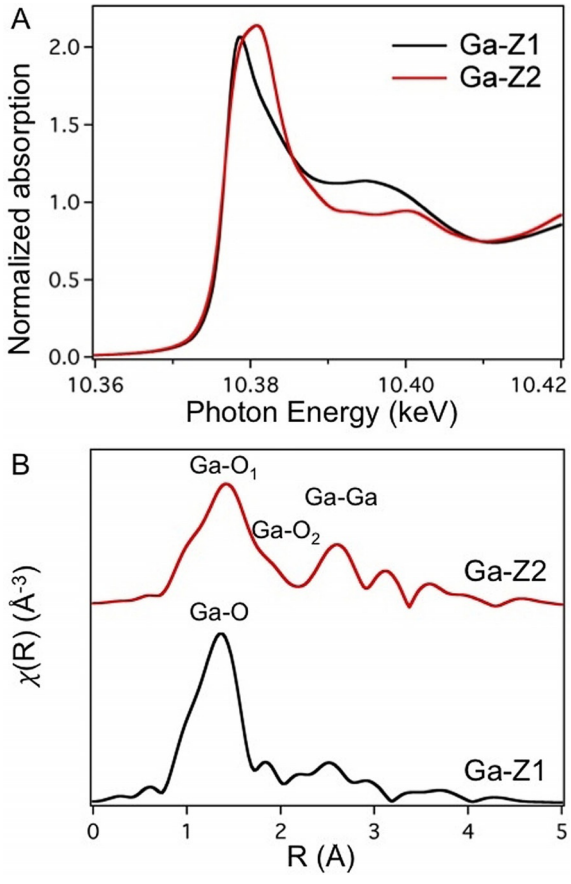

Figure 1. A) Normalized Ga K-edge XANES spectra for H-Ga-ZSM-5 zeolites prepared by different methods: Ga-Z1 (direct synthesis) and Ga-Z2 (solution ion exchange). B) Fourier transform magnitudes of k^2-weighted Ga K-edge EXAFS spectra of Ga-Z1 and Ga-Z2 (using the k range: 2–12 $Å^{-1}$). Peaks are labelled with Ga species corresponding to the fit results in Tables 2 and S2. All the measurements are taken at ambient temperature.

2–4 Å in the spectrum of Ga-Z2, indicate the local environments around Ga atoms in these two zeolites are different. In particular, we observe better defined structure of more distant atomic species around Ga in Ga-Z2 compared to Ga-Z1, consistent with the hypothesis that Ga_xO_y species dominate in the former sample, while Ga is in the zeolite framework in the latter one. To extract detailed local structure information from both samples, quantitative analysis of their EXAFS spectra was carried out. The fitting results (Table 2 and Figure S5) highlight distinct differences in the local environments around Ga atoms in these samples, in agreement with visual observations of XANES and EXAFS data (vide supra). The coordination number of the Ga–O bond in Ga-Z1 is close to four, consistent with a tetrahedral-coordination of Ga atoms with an effective Ga-O distance of 1.81 ± 0.01 Å. This value falls within the range reported in literature[11a] and is close to the valus measured for Ga-Z2 and Ga-Z3 (Table S2). The best fit for Ga-Z2 involves two distinct Ga-O shells with interatomic distances of 1.90 ± 0.02 Å and 2.11 ± 0.08 Å. Such a split in the Ga-O distances is likely due to the distribution of Ga atoms between tetrahedral and octahedral sites.[23] We estimate the fraction of tetrahedral Ga sites in Ga-Z2 to be 80% (refer to the Supporting Information for detailed calculations). The peak at about 2.97 Å is attributed to Ga-Ga pairs.

Table 2: Best fits of the structural parameters obtained from Ga K-edge EXAFS.

Sample	Pair	*N*	*R* [Å]	σ^2 [Å^2]
Ga-Z1	Ga-O	4.2 ± 0.4	1.81 ± 0.01	0.005 ± 0.001
Ga-Z2	Ga-O_1	3.4 ± 0.9	1.90 ± 0.02	0.006 ± 0.004
	Ga-O_2	1.3 ± 0.8	2.11 ± 0.08	0.006 ± 0.004
	Ga-Ga	8.5 ± 3.8	2.97 ± 0.03	0.017 ± 0.005

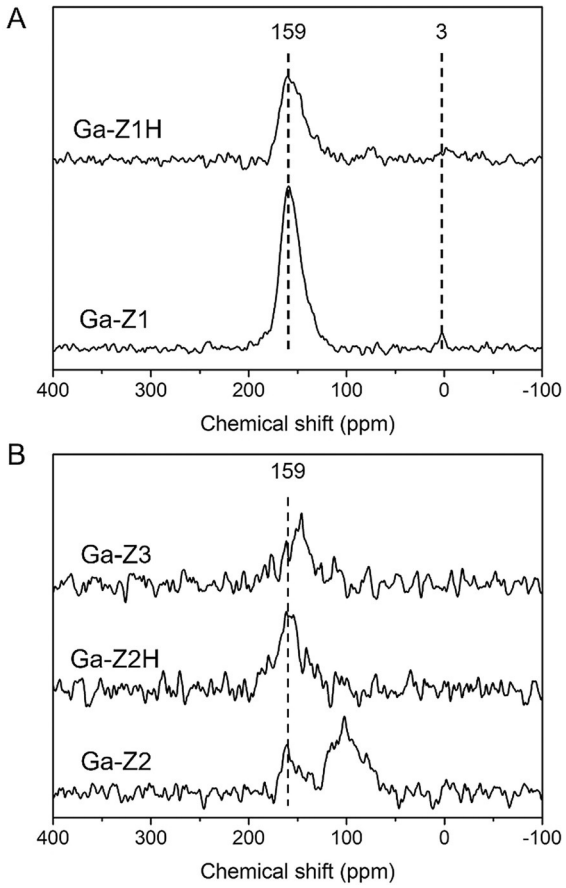

Figure 2. A) ^{71}Ga MAS NMR spectra of hydrated Ga-ZSM-5 zeolites prepared via direct synthesis (Ga-Z1) and after H_2 treatment (Ga-Z1H). B) Spectra of hydrated Ga-ZSM-5 zeolite samples via other preparation methods: Ga-Z2 (solution ion exchange), Ga-Z2H (Z2 after H_2 treatment), and Ga-Z3 (chemical vapor-phase exchange). See Figure S6 for an overlay of all spectra.

The effect of Ga-ZSM-5 sample preparation on the coordination (or local environment) of Ga species was assessed by solid-state NMR. Previous studies of ^{71}Ga MAS NMR spectra generally assign peaks in the ranges 150–160 ppm and −7–12 ppm to tetrahedral (framework) Ga_{FW} and octahedral (extra-framework) Ga_{EFW} (i.e. Ga_xO_y), respectively.[24] However, an alternative interpretation from Dai et al.[25] is that the signal at 150–160 ppm is a tetrahedral coordination attributed to either Ga_{FW} cations or Ga_{EFW} species such as Ga^{3+}, $[Ga(OH)_2]^+$, or [GaO(OH)]. Moreover, Gao et al.[3a] assigned the peak at 58 ppm to highly dispersed Ga_xO_y particles, and the peak at 190 ppm to cationic $[GaO]^+$ or its hydrous state $[Ga(OH)_2]^+$. The ^{71}Ga MAS NMR spectra of all Ga-ZSM-5 samples in this study are shown in Figure 2. Samples Ga-Z1 and Ga-Z1H exhibit a single peak around 159 ppm (Figure 2A), indicating the majority of Ga species have a tetrahedral coordination. For the remaining samples (Figure 2B), the signal-to-noise ratio of spectra is relatively low due to the strong broadening effect on the oxidic extra-framework Ga species.[24c] The Ga-Z2 spectrum contains two bands located at 159 and 102 ppm, respectively. Since EXAFS suggests 80% of the Ga sites in Ga-Z2 are tetrahedrally coordinated, the peak at 102 ppm could be assigned to distorted tetrahedral sites within extra-framework Ga or amorphous Ga_xO_y. After H_2 treatment, the peak located at 102 ppm disappears due to the formation of dispersed tetrahedral $[Ga(X)_2]^+$ (X = OH or H) species that can exchange with Brønsted acid sites. Indeed, the NMR spectrum for Ga-Z2H (Figure 2B) is similar to that of Ga-Z3 (i.e. single peak around 147 ppm), which is consistent with tetrahedrally-coordinated Ga reported by Bell.[11a] Direct comparison of these two spectra with that of Ga-Z1 provides evidence for the presence of framework Ga in the latter (although the exact percentage cannot be quantified). The presence of framework Ga in sample Ga-Z1 (and Ga-Z1H) is inferred from the large difference in signal-to-noise ratio compared to Ga-Z2 and Ga-Z3, despite all samples having nearly identical Ga concentration (Table 1). The presence of tetrahedrally-coordinated Ga_{FW} leads to higher local symmetry (i.e. higher peak intensity, Figure S6), consistent with previous ^{71}Ga NMR spectra of gallosilicates,[24a,26] whereas the asymmetrical environment of tetrahedral $[Ga(X)_2]^+$ species leads to lower signal-to-noise ratios.

The ^{71}Ga MAS NMR spectra of samples Ga-Z1, -Z1H, -Z2H, and -Z3 indicate a predominance of tetrahedral Ga

species, which could be either $[GaX_2]^+$ (Scheme 1E) or $[GaH]^{2+}$ (Scheme 1F). The relatively high Si/Al ratio of H-ZSM-5 samples suggests there are few paired Al sites, which would limit the number of $[GaH]^{2+}$ species; thus, we propose the majority of extra-framework sites are $[GaX_2]^+$. Direct synthesis of Ga-Z1 generates $[Ga(OH)_2]^+$ in the as-synthesized product. High temperature hydrogen treatment of sample Ga-Z1H is expected to result in sequential hydrogen exchange steps leading to the overall reaction

$$[Ga(OH)_2]^+ + 2\,H_2 \leftrightarrow [GaH_2]^+ + 2\,H_2O \quad (1)$$

Comparison of XAFS data for Ga-Z1 and Ga-Z1H (Figure S7) reveals no shift in spectra. A similar analysis of Ga-Z2 and Ga-Z2H (Figure S8) reveals only subtle differences in XAFS spectra which may reflect the loss of distorted tetrahedral sites (consistent with ^{71}Ga MAS NMR). Treatment of Ga-Z2 with H_2 also has the potential to mobilize Ga_xO_y to generate dispersed $[GaH_2]^+$ sites via a similar reaction,

$$Ga_xO_y + x\,[H]^+ + (x/2+y)\,H_2 \leftrightarrow x\,[GaH_2]^+ + y\,H_2O \quad (2)$$

An additional hydrogen exchange generates a Brønsted acid site and GaH_3, which we consider to be the short-lived, mobile species during hydrogen treatment. DFT calculated free energy changes and activation barriers for the sequential transformation of $[Ga(OH)_2]^+$ to GaH_3 are provided in Table S3. The final step of treatment involves exposure to O_2 at high temperature, which reoxidizes sites to $[Ga(OH)_2]^+$. During catalyst testing, non-oxidative DHA of ethylene produces H_2 to regenerate $[GaH_2]^+$ species in situ, which we presume herein to be the active site for Lewis acid catalysis.

The catalytic performance of all H-Ga-ZSM-5 catalysts were compared in the ethylene DHA reaction using a packed bed reactor with a fixed space velocity (3000 mL g^{-1} h^{-1}) and ethylene partial pressure (12.7 kPa). Reactions were performed at sub-complete ethylene conversion (ca. 80%) to assess catalyst deactivation and selectivity towards light olefins and aromatics. As shown in Figure 3A, isoconversion comparisons reveal the following order of aromatic selectivity: Ga-Z1H > Ga-Z1 ≈ Ga-Z2H > Ga-Z3 > Ga-Z2 > Z-ref. Commercial ZSM-5 (Z-ref), which lacks Ga_{EFW} Lewis acid sites (LASs), exhibits the least aromatic selectivity (16%) owing to the presence of Brønsted acid sites (BASs) that preferentially direct the formation of alkanes (e.g. 13% butane) and olefins (e.g. 23% propylene, 19% butylenes). Among H-Ga-ZSM-5 catalysts, Ga-Z2 has the lowest aromatics selectivity owing to the presence of distorted $[GaH_2]^+$ sites or Ga_xO_y species on the zeolite surface, which are reportedly inert sites for aromatic formation.[10] The Ga-Z3 catalyst obtained via chemical vapor phase exchange produced an appreciable amount of aromatics (45%), suggesting the existence of well-dispersed Ga_{EFW} species (i.e. isolated $[GaH_2]^+$ sites substituting Brønsted acids as illustrated in Scheme 1E with T = Al).[11a] The catalyst prepared via direct synthesis (Ga-Z1) exhibits higher aromatics selectivity (52%), which can be correlated to the presence of tetrahedrally-coordinated Ga^{3+} species. Analyses by XAFS and ^{71}Ga MAS NMR cannot distinguish the fraction of tetrahedrally-coordinated Ga occupying framework and extra-framework sites, which are illustrated in Scheme 1A and E, respectively. One differentiating factor between samples Ga-Z3 and Ga-Z1 is that Ga_{EFW} in the latter can be associated with either Al_{FW} or Ga_{FW} in the framework. Another factor that must be considered is the potential impact of framework Ga on the acidity of BASs. Investigation of both scenarios by DFT modeling is described later.

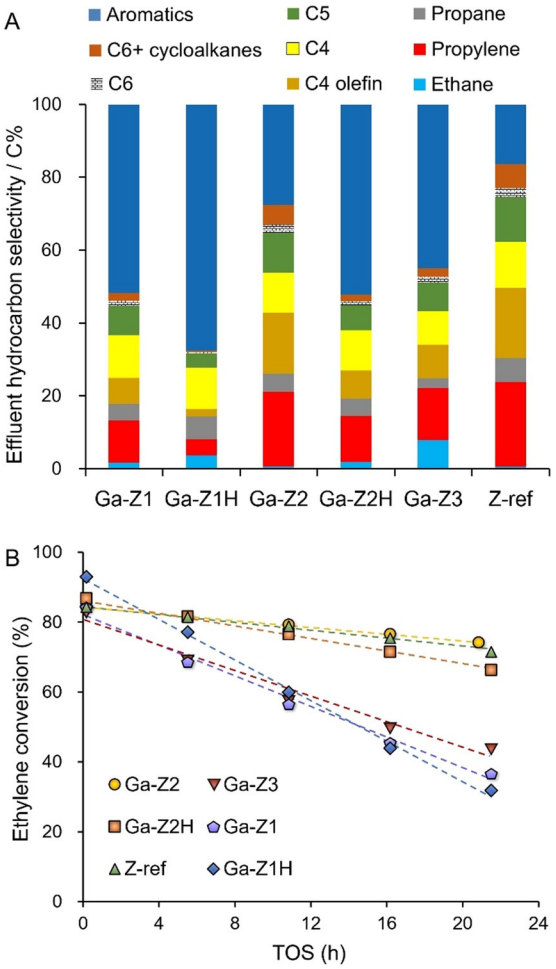

Figure 3. A) Hydrocarbon product selectivity in the ethylene DHA reaction over various H-form ZSM-5 catalysts (Ga-Z1, Ga-Z1H, Ga-Z2, Ga-Z2H, Ga-Z3, and Z-ref) at 400°C, 1 atm, and isoconversion of ethylene (ca. 80%). The space velocity was fixed at 3000 mL g^{-1} h^{-1} using a feed pressure of 12.7 kPa ethylene and 88.6 kPa argon. Data were acquired after 10 min time on stream (TOS) with a carbon balance >96%, which is listed in Table S4 for each catalyst along with detailed product selectivity for a broader class of compounds in the effluent stream. Changes in product selectivity with increasing TOS are shown in Figure S10. B) Ethylene conversion for each catalyst at the same reaction conditions as a function of TOS. Dashed lines are linear regression showing two groups with lower and higher rates of deactivation (slopes with absolute values of 0.7 ± 0.2 and 2.3 ± 0.5 h^{-1}, respectively).

Figure 3A compares product selectivities for specific light paraffins and olefins where the most notable differences observed among the catalysts are with respect to propylene

and C_4 olefins. Comparisons were made at a fixed space velocity, where we observe nearly identical ethylene conversion at initial time on stream (Figure 3B), indicating all six catalysts have similar activity. Comparison of the rates of catalyst deactivation reveal two groups of similar stability: those with lower rates of deactivation (Ga-Z2, Ga-Z2H, and Z-ref) and those with 3.4-fold higher rates of deactivation (Ga-Z1, Ga-Z1H, and Ga-Z3). With respect to the accelerated rates of deactivation for Ga-Z1 and Ga-Z3, this may be attributed in part to their higher percentages of extra-framework Al (Table 1). For Ga-Z3 these species are the result of dealumination during H_2 treatment, which leads to framework defects that are evident in XAFS analysis (Figure S9).

Hydrogen treatment leads to significant increases in aromatics production for both Ga-Z1 and Ga-Z2. Prior studies have shown that the reduction of Ga-zeolites in H_2 at high temperature is essential to reduce Ga_xO_y [Eq. (2)] to more dispersed Ga species.[11b,12] It has also been reported that reoxidation to the Ga^{3+} phase after dispersion can further enhance aromatic selectivity, indicating reoxidized Ga differs from the initial Ga_xO_y species. This is consistent with the observation of Ga-Z2 (containing Ga_xO_y species) producing fewer aromatics than Ga-Z2H (after H_2 treatment). Indeed, the BTX selectivity increases from 17 to 39% (Figure 4), indicating a large shift to well-dispersed Ga^{3+} species, consistent with its NMR spectrum (Figure 2B). It was anticipated that Ga-Z3, which also contains Ga^{3+} species (Figure S9 and Table S2) and was treated with H_2, would perform similarly to Ga-Z2H; however, we observe the former produces 7% less BTX. This may be attributed, in part, to the loss of framework Al in Ga-Z3 during chemical vapor phase exchange. An even more unexpected observation was the fact that H_2 treatment of Ga-Z1 raises its BTX selectivity from 36 to 53% (Figure 4, sample Ga-Z1H), the highest among all samples tested. The ^{71}Ga MAS NMR spectra for samples before and after treatment are identical (Figure 2A). Moreover, ^{27}Al MAS NMR reveals no loss of framework Al species with H_2 treatment, and only a small (ca. 2%) reduction in the amount of extra-framework Al (Table 1). The exact reasoning for the large increase in aromatics yield is not fully understood, but herein we put forth a hypothesis invoking preferential siting of BAS and LAS near Al_{FW} and Ga_{FW}, noting that Ga-Z1 is the only sample that features Ga_{FW} sites.

Ethylene can potentially be activated on a BAS or LAS,[6d] and we present the most likely pathways for each case at the framework tetrahedral T12 site in Figure 5A (additional pathways explored by DFT are compiled in Table S5). Despite challenges in measuring[27] or calculating[28] intrinsic acid strengths, it has been experimentally and theoretically shown[29,30] that Al_{FW} results in a BAS with stronger intrinsic acidity than Ga_{FW}; therefore, the presence of Ga_{FW} in sample Ga-Z1 is expected to weaken the intrinsic strength of BASs, which can impact the catalytic mechanisms underlying ethylene DHA. To examine differences among heteroatom

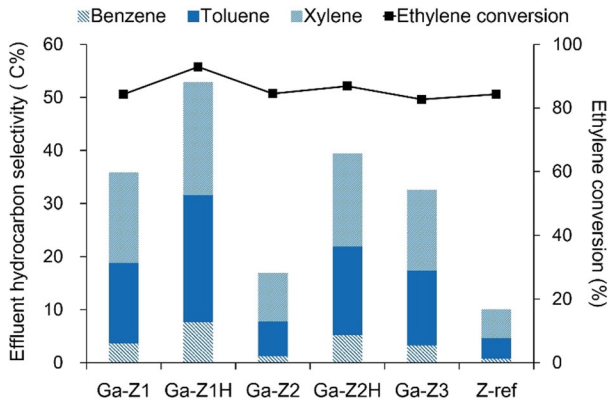

Figure 4. Comparison of aromatics products for H-Ga-ZSM-5 catalysts before (Ga-Z1, Ga-Z2) and after (Ga-Z1H, Ga-Z2H, Ga-Z3) H_2 treatment compared to the reference H-ZSM-5 catalyst (Z-ref). Here we report the BTX selectivities (histogram, left *y*-axis) and ethylene conversion (square symbols, right *y*-axis) for the ethylene DHA reaction at 400 °C and 1 atm. The space velocity was fixed at 3000 mL g^{-1} h^{-1}, and the feed pressure was composed of 12.7 kPa ethylene and 88.6 kPa argon. Data were acquired after 10 min time on stream.

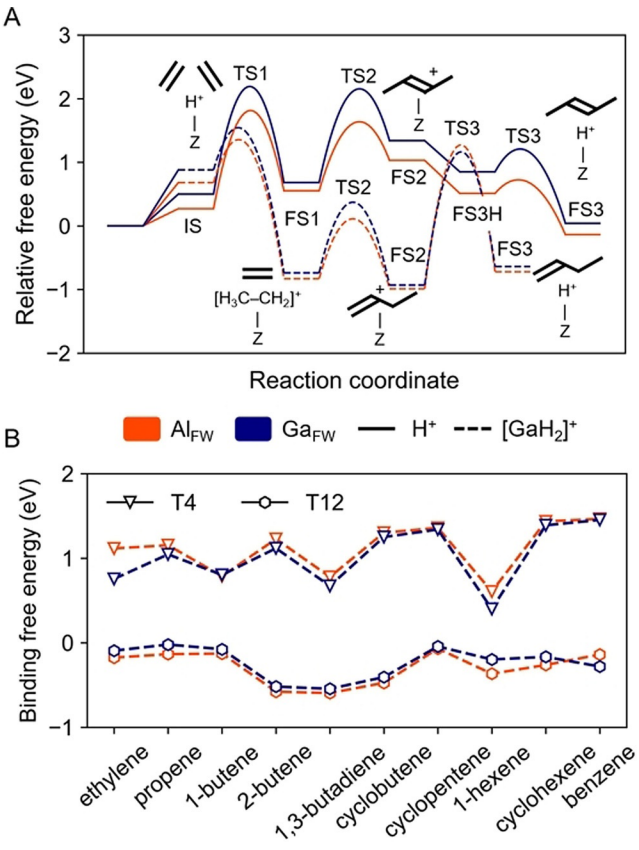

Figure 5. Calculated properties of H^+ Brønsted acid sites and $[GaH_2]^+$ Lewis acid sites near an Al_{FW} (orange) or Ga_{FW} (blue) heteroatom at the T12 site of MFI. A) Free energy diagram for ethylene activation and oligomerization to 2-butene at an H^+ site, and 1-butene at a $[GaH_2]^+$ site (similar calculations for Ga^+ are provided in Figure S12). B) Binding free energies of unsaturated hydrocarbons (i.e. olefins and aromatics) at $[GaH_2]^+$ Lewis acid sites in the T4 (triangles) and T12 (circles) positions (corresponding calculations at Brønsted acid sites are shown in Figure S13.). All free energies are reported at 400 °C and standard pressure for each gas phase species.

sites, we explored the activation and oligomerization of ethylene to butene (a characteristic product of the DHA reaction) by means of periodic DFT calculations with van der Waals (vdW) corrections. To this end, we selected the T12 site of ZSM-5 as a representative BAS (and one of the most frequently studied in literature), located at the intersection of straight and sinusoidal channels in the MFI structure.[28] The free energy diagram depicting the energies of reaction and activation barriers for each intermediate step for Al_{FW} in orange and Ga_{FW} in blue at 400 °C and standard pressure, are shown in Figure 5 A. Visualizations of the initial, transition, and final states along the reaction coordinate are provided in Figure S11.

At 400 °C, ethylene is stabilized at the vicinity of the BAS through vdW forces and π-bonds with a total free binding energy of 0.06 eV for Al_{FW} and 0.10 eV for Ga_{FW}. The activation of ethylene at a BAS proceeds with the formation of a positively-charged ethyl ($C_2H_5^+$) species (Figure S11, top) with free activation barriers of 1.54 eV (Al_{FW}) and 1.68 eV (Ga_{FW}). Next, a second ethylene molecule attacks the unsaturated carbon atom of the ethyl group and proceeds through the formation of a π-bonded transition state, forming a butyl ($C_4H_9^+$) complex (Figure S11, middle). The free activation barrier for this step was calculated to be 1.07 eV (Al_{FW}) and 1.45 eV (Ga_{FW}) and is followed by an exergonic internal hydrogen transfer step. The formation of 2-butene and restoration of the BAS occurs by β-hydrogen elimination with an activation barrier of 0.16 and 0.31 eV for Al_{FW} and Ga_{FW}, respectively (Figure S11, bottom). We also considered the formation of 1-butene with Al_{FW}, which was only marginally more activated. Overall, each BAS provides an accessible pathway to the activation and oligomerization of ethylene to butene; however, the barriers of all elementary steps are somewhat lower when the framework heteroatom is Al instead of Ga, suggesting that the BAS bound to Al_{FW} is more amenable to oligomerization or hydrocarbon upgrade reactions. This result is consistent with the higher intrinsic acidity of H-(Al)-ZSM-5 compared to H-(Ga)-ZSM-5.[30,31]

Zeolite samples Ga-Z1, -Z2, and -Z3 all contain Ga_{EFW} sites with Lewis acidity that affects the overall catalytic activity and product selectivity. To examine the role of Ga_{EFW} we built on the work by Bell and co-workers[18e] to study the oligomerization of ethylene to 1-butene over $[GaH_2]^+$ sites bound to framework Al_{FW} and Ga_{FW} anionic sites. The reaction free energies and activation barriers of the accessible pathway for ethylene oligomerization for $[GaH_2]^+$ (dotted line) are visualized in Figure 5 A. For comparison we also include an analysis of Ga^+ species, as well as various other inaccessible pathways we considered for the activation of ethylene in the Supporting Information (Figure S12 and Table S5). The activation of ethylene on $[GaH_2]^+$ results in a $[C_2H_5\text{-}GaH]^+$ intermediate, resembling the activation mechanism on the BAS, but with a lower ethylene activation free energy on the $[GaH_2]^+$ LAS. For instance, calculations with Al_{FW} reveal an activation barrier of only 0.62 eV at the LAS compared to 1.54 eV at the BAS. In the case of Ga_{FW}, the free barrier at the LAS is only 0.61 eV, but 1.68 eV at the BAS. For both framework heteroatoms, the coupling to a second ethylene molecule to form $[C_4H_9\text{-}GaH]^+$ is exergonic and fast. Following this low energy pathway to C–C coupling on $[GaH_2]^+$ is a β-hydride elimination step restoring the LAS and forming 1-butene. The free energy barriers we found were 2.26 eV for Al_{FW} and 2.10 eV for Ga_{FW}. Given the large barrier of this final step, one might argue that it is rate-limiting. In that case, our results suggest that Ga_{FW} is beneficial, given that the barrier to restore the Ga_{FW}-BAS is 0.16 eV lower than restoring the Al_{FW}-BAS. This is again consistent with Al_{FW}-BAS having a higher intrinsic acidity, and therefore rendering Ga_{FW} the stronger conjugated base.

Extra-framework Ga_{EFW} may play a critical role in increasing the selectivity to aromatics,[6d] but since complete aromatization pathways are complex and highly branched, it is not possible to rigorously examine them with DFT. Instead, we have calculated the binding free energies of various olefins and aromatics to BAS and $[GaH_2]^+$ extra-framework sites located at Al_{FW} and Ga_{FW} heteroatoms in the T12 and T4 positions (numerical values in Tables S6 and S7) representing tetrahedral (T) sites of the MFI crystal structure located within straight (i.e. intersection) and sinusoidal channels, respectively. These unsaturated hydrocarbons shown in Figure 5 B have been detected in catalytic experiments (Figure 3), and their binding free energies show no significant sensitivity to the identity of the framework heteroatom. We observed, however, that binding to the $[GaH_2]^+$ site in the T4 position located within the sinusoidal channel is highly unfavorable. In contrast, the difference between T4 and T12 when only a BAS is present, is much less pronounced (Figure S13). Hence, these calculations suggest the presence of $[GaH_2]^+$ in sinusoidal channels alters diffusion characteristics, which in turn can impact shape selectivity by directing transport largely through less tortuous straight channels.

During H_2 treatment we noted that extra-framework Ga_{EFW} becomes mobile and can be atomically dispersed to increase aromatics selectivity.[11] One of the unexplained observations in Figure 4 is the dramatic enhancement of aromatics selectivity over Ga-Z1 after H_2 treatment. Here we hypothesize that the enhanced BTX selectivity is due to a redistribution of extra-framework $[GaH_2]^+$ among available framework Al_{FW} and Ga_{FW} sites. While our DFT results are inconclusive regarding the role of framework heteroatoms on selectivity, we aim to rationalize the substantial selectivity improvement observed for Ga-Z1H by calculating the free energies associated with swapping a proton at a Ga_{FW} framework site (labelled as T_i) with $[GaH_2]^+$ at an Al site (labelled as T_j), which is expressed in the following reaction

$$H^+\text{–}Ga_{FW}(T_i) + [GaH_2]^+\text{–}Al_{FW}(T_j) \rightarrow [GaH_2]^+\text{–}Ga_{FW}(T_i) + H^+\text{–}Al_{FW}(T_j) \quad (3)$$

Here, we considered $[GaH_2]^+$ to be the more likely Ga_{EFW} species under hydrogen treatment conditions. The ion-exchange energies for all possible T-site combinations are summarized in Figure 6, where blue rectangles indicate a preference for a $[GaH_2]^+$ LAS located near framework Ga_{FW} and a strong BAS near Al_{FW}. This arrangement is generally preferred for Ga_{FW} in the T1, T2, T6, T7, T8, and T11 positions. In contrast, the almost exclusively red rectangles for Ga_{FW} at T10, and their prevalence in the rows for

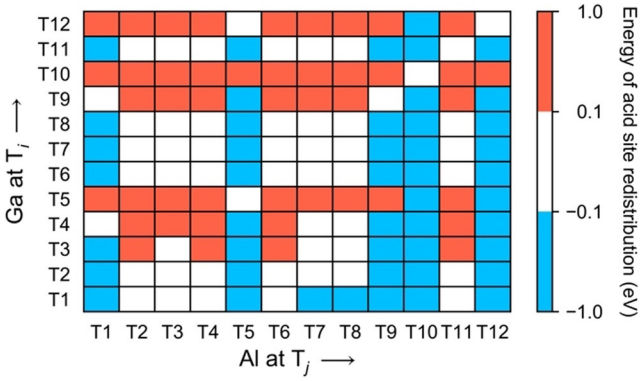

Figure 6. Brønsted (H^+) and Lewis ($[GaH_2]^+$) acid site exchange energies between framework Ga_{FW} at T_i sites and Al_{FW} atoms at T_j sites at 500 °C according to the reaction in Equation (3). Blue rectangles indicate that the $[GaH_2]^+$ Lewis acid is more stable near a Ga_{FW} and the Brønsted acid site forms near Al_{FW}. For combinations with white rectangles the preference for $[GaH_2]^+$ to form near Ga_{FW} or Al_{FW} is negligible.

Ga_{FW} at T5, T9, and T12 positions suggests that a BAS is more likely on Ga_{FW} in these locations. The corresponding calculated values are provided in Table S8.

It is plausible that mobilizing Ga_{EFW} species during H_2 treatment can indeed alter the BAS/LAS site distribution, but without knowledge of the exact distribution of framework Al_{FW} and Ga_{FW} sites in sample Ga-Z1, it is not possible to draw a firm conclusion regarding the BAS/LAS distribution; however, the calculated BAS/LAS site preferences along with the demonstrated improvement of ethylene conversion and selectivity to aromatics of Ga-Z1H support the hypothesis that H_2 treatment of Ga-Z1 leads to a beneficial redistribution of BAS/LAS sites. It should also be noted that this is fully consistent with ^{71}Ga MAS NMR and XAFS data (Figures 2 A and S7, respectively) showing no apparent change in spectra before and after H_2 treatment, which suggests that LAS speciation remains the same.

An underlying characteristic of catalysts Ga-Z1, -Z2H, and -Z3 is the presence of $[GaH_2]^+$ extra-framework LAS species, which is a likely explanation for their nearly identical performance in DHA of ethylene. LAS/Ga_{FW} combinations can only be achieved in Ga-Z1 (the direct synthesis method) given its distinguishing attribute of having Ga_{FW} heteroatoms substituted at framework sites. These sites may ultimately be responsible for improved BTX selectivity, but conclusive evidence remains elusive. The notable improvement of Ga-Z1 performance after H_2 treatment (sample Ga-Z1H) can be rationalized by the calculated differences in stability for forming BAS and LAS sites near Al_{FW} and Ga_{FW} sites. It is plausible that the high temperature of H_2 treatment coupled with the mobility of $[GaH_2]^+$ species can lead to this exchange of sites; however, in order for this to be true, it implies that direct synthesis of Ga-Z1 places an appreciable fraction of extra-framework Ga_{EFW} at locations that are on average less energetically favorable. Although the exact location and quantity of framework and extra-framework Ga sites cannot easily be resolved, it is frequently reported that zeolite synthesis produces metastable, or kinetically trapped, structures; and with sufficiently high temperature it is possible to promote interzeolite transformations from the initial structure to one that is more thermodynamically stable.[33] A similar phenomenon may occur for Ga_{EFW} species during H_2 treatment to result in a more energetically favorable distribution of sites. This hypothesis, although unverifiable by the techniques used in this study, is consistent with experimental and modeling results, and thus is a viable explanation for the superior performance of Ga-Z1H.

Conclusion

We present a direct synthesis method to introduce well-dispersed extra-framework Ga^{3+} Lewis acid sites without the need for additional post-synthetic treatments (i.e. solution ion exchange or chemical vapor deposition). A combination of advanced characterization techniques such as XAFS and solid-state NMR spectroscopy indicates that framework Ga_{FW} and tetrahedrally-coordinated extra-framework Ga_{EFW} sites can be simultaneously generated via this direct synthesis method. We also investigate the roles of Ga speciation in ZSM-5 prepared by three distinct methods, direct synthesis (Ga-Z1), solution ion exchange (Ga-Z2), and chemical vapor-phase exchange (Ga-Z3), to identify the structure and catalytic function of different Ga sites. We have shown that any type of Ga_{EFW} Lewis site can promote the formation of BTX with a total selectivity as high as 53 %, whereas the BTX selectivity is only 10 % for commercial H-ZSM-5 at comparable ethylene conversion. Isoconversion comparisons further reveal the following order of aromatic selectivity: Ga-Z1 > Ga-Z3 > Ga-Z2, indicating the Ga Lewis sites and the existence of framework Ga_{FW} species in Ga-Z1 catalyst lead to superior catalytic performance and promote the formation of aromatics. XAFS and NMR measurements both indicate Ga-Z2 prepared via solution ion exchange contains a large amount of either distorted $[GaX_2]^+$ or Ga_xO_y species on the external zeolite surface, suggesting that these species are not the most active Lewis sites for aromatics promotion.

We further explore the effect of H_2 treatment on Ga-Z1 and Ga-Z2 and directly compare their selectivity with Ga-Z3, which was obtained via chemical vapor-phase exchange involving H_2 treatment. For both treated Ga-Z1H and Ga-Z2H catalysts, we observed increased BTX selectivity, but the improvement was attributed to two different phenomena: For Ga-Z2 the H_2 treatment disperses inactive Ga to active $[GaH_2]^+$ species, while for Ga-Z1 the H_2 treatment is believed to redistribute Brønsted acid protons to Al_{FW} and $[GaH_2]^+$ to select Ga_{FW} sites. The Brønsted and Lewis acid site redistribution is supported by DFT simulations, which also suggest that stronger H^+/Al_{FW} sites lower barriers for ethylene dimerization over BAS, while the stronger conjugated base sites with Ga_{FW} may favor slow deprotonation steps. DFT calculations also indicate possible changes in diffusion characteristics with placement of Ga_{EFW} in sinusoidal channels, which may alter shape selectivity. Jointly, these results would explain the exceptional activity and selectivity to aromatics observed for the Ga-Z1H sample. To our knowledge, few studies have considered the possibility of directing

Lewis acid siting in zeolites (i.e. the majority focus on Al_{FW} siting and distribution[34]). Our findings indicate that if heteroatoms (such as Ga) can be selectively placed at specific T sites within zeolites, this would afford the opportunity to direct the spatial distribution of Lewis acid sites for bifunctional catalysis.

Acknowledgements

J.D.R. and L.C.G. received financial support from the National Science Foundation (Award CBET-1512224). J.D.R. received additional support from the Welch Foundation (Award E-1794). H.T. was supported by the U.S. Department of Energy (DOE), Office of Science, Office of Basic Energy Sciences under award number DE-SC0011983 to carry out DFT simulations. XAFS analysis work of AIF was supported in part by the Catalysis Center for Energy Innovation, an Energy Frontier Research Center funded by the U.S. Department of Energy, Office of Science, Office of Basic Energy Sciences under Award No. DE-SC0001004. J.L. was supported in part by the U.S. Department of Energy, Office of Science, Office of Workforce Development for Teachers and Scientists (WDTS) under the Visiting Faculty Program (VFP). This Research used beamline 7-BM (QAS) of the National Synchrotron Light Source II, a U.S. DOE Office of Science User Facility operated for the DOE Office of Science by Brookhaven National Laboratory (BNL) under Contract No. DE-SC0012704. We acknowledge Dr. S. Ehrlich for collecting XAFS data at the QAS beamline and Dr. N. Marinkovic for help with beamline measurements. Beamline operations were supported in part by the Synchrotron Catalysis Consortium (U.S. DOE, Office of Basic Energy Sciences, Grant No. DE-SC0012335). This work used the Extreme Science and Engineering Discovery Environment (XSEDE) Stampede2 at the Texas Advanced Computing Center through allocation TG-CHE140109, which is supported by National Science Foundation grant number ACI-1548562.[35] We also used resources of the National Energy Research Scientific Computing Center (NERSC), a U.S. Department of Energy Office of Science User Facility operated under Contract No. DE-AC02-05CH11231, and the uHPC cluster managed by the University of Houston and acquired through NSF Award Number 1531814. Finally, we acknowledge the use of the Maxwell/Opuntia/Sabine Cluster and HPC support from Keith Crabb and Jeffrey Sarlo at the University of Houston.

Conflict of interest

The authors declare no conflict of interest.

Keywords: acid siting · aromatics · bifunctional catalysis · Lewis acid · zeolite synthesis

[1] a) H.-G. Franck, J. W. Stadelhofer, *Industrial Aromatic Chemistry*, Springer, Heidelberg, **1988**; b) K. W. H.-J. Arpe, *Industrial Organic Chemistry*, Fourth Edition, Wiley-VCH, Weinheim, **2008**.

[2] X. Yang, X. Su, D. Chen, T. Zhang, Y. Huang, *Chin. J. Catal.* **2020**, *41*, 561 – 573.

[3] a) P. Gao, Q. Wang, J. Xu, G. Qi, C. Wang, X. Zhou, X. Zhao, N. Feng, X. Liu, F. Deng, *ACS Catal.* **2018**, *8*, 69 – 74; b) P. Gao, J. Xu, G. Qi, C. Wang, Q. Wang, Y. Zhao, Y. Zhang, N. Feng, X. Zhao, J. Li, F. Deng, *ACS Catal.* **2018**, *8*, 9809 – 9820.

[4] a) S. Ma, X. Guo, L. Zhao, S. Scott, X. Bao, *J. Energy Chem.* **2013**, *22*, 1 – 20; b) P. Schwach, X. Pan, X. Bao, *Chem. Rev.* **2017**, *117*, 8497 – 8520.

[5] a) Y. Ono, K. Osako, G. J. Kim, Y. Inoue in *Studies in Surface Science and Catalysis*, *Vol. 84* (Eds.: J. Weitkamp, H. G. Karge, H. Pfeifer, W. Hölderich), Elsevier, Amsterdam, **1994**, pp. 1773 – 1780; b) P. Qiu, J. H. Lunsford, M. P. Rosynek, *Catal. Lett.* **1998**, *52*, 37 – 42; c) V. R. Choudhary, P. Devadas, S. Banerjee, A. K. Kinage, *Microporous Mesoporous Mater.* **2001**, *47*, 253 – 267; d) Y. Ono, T. Baba, *Phys. Chem. Chem. Phys.* **2015**, *17*, 15637 – 15654.

[6] a) L. A. Dufresne, R. Le Van Mao, *Catal. Lett.* **1994**, *25*, 371 – 383; b) H. Coqueblin, A. Richard, D. Uzio, L. Pinard, Y. Pouilloux, F. Epron, *Catal. Today* **2016**, *289*, 62 – 69; c) X. Chen, M. Dong, X. Niu, K. Wang, G. Chen, W. Fan, J. Wang, Z. Qin, *Chin. J. Catal.* **2015**, *36*, 880 – 888; d) M.-F. Hsieh, Y. Zhou, H. Thirumalai, L. C. Grabow, J. D. Rimer, *ChemCatChem* **2017**, *9*, 1675 – 1682.

[7] a) A. Bhan, W. N. Delgass, *Catal. Rev.* **2008**, *50*, 19 – 151; b) S.-W. Choi, W.-G. Kim, J.-S. So, J. S. Moore, Y. Liu, R. S. Dixit, J. G. Pendergast, C. Sievers, D. S. Sholl, S. Nair, C. W. Jones, *J. Catal.* **2017**, *345*, 113 – 123; c) M. W. Schreiber, C. P. Plaisance, M. Baumgärtl, K. Reuter, A. Jentys, R. Bermejo-Deval, J. A. Lercher, *J. Am. Chem. Soc.* **2018**, *140*, 4849 – 4859; d) N. M. Phadke, E. Mansoor, M. Bondil, M. Head-Gordon, A. T. Bell, *J. Am. Chem. Soc.* **2018**, *141*, 1614 – 1627.

[8] C. D. Gosling, D. A. Hamm (Honeywell UOP LLC), US 5258563 A, **1992**.

[9] a) A. A. Gabrienko, S. S. Arzumanov, A. V. Toktarev, D. Freude, J. Haase, A. G. Stepanov, *J. Phys. Chem. C* **2011**, *115*, 13877 – 13886; b) S. Yasumura, M. Huang, X. Wu, C. Liu, T. Toyao, Z. Maeno, K.-i. Shimizu, *Catal. Today* **2019**, *352*, 118 – 126.

[10] J. F. Joly, H. Ajot, E. Merlen, F. Raatz, F. Alario, *Appl. Catal. A* **1991**, *79*, 249 – 263.

[11] a) N. M. Phadke, J. Van der Mynsbrugge, E. Mansoor, A. B. Getsoian, M. Head-Gordon, A. T. Bell, *ACS Catal.* **2018**, *8*, 6106 – 6126; b) K. M. Dooley, C. Chang, G. L. Price, *Appl. Catal. A* **1992**, *84*, 17 – 30; c) V. R. Choudhary, A. K. Kinage, C. Sivadinarayana, S. D. Sansare, M. Guisnet, *Catal. Lett.* **1995**, *33*, 401 – 412.

[12] G. L. Price, V. Kanazirev, *J. Catal.* **1990**, *126*, 267 – 278.

[13] M. W. Schreiber, C. P. Plaisance, M. Baumgärtl, K. Reuter, A. Jentys, R. Bermejo-Deval, J. A. Lercher, *J. Am. Chem. Soc.* **2018**, *140*, 4849 – 4859.

[14] a) N. Al-Yassir, M. N. Akhtar, S. Al-Khattaf, *J. Porous Mater.* **2012**, *19*, 943 – 960; b) V. R. Choudhary, S. A. R. Mulla, S. Banerjee, *Microporous Mesoporous Mater.* **2003**, *57*, 317 – 322; c) V. R. Choudhary, P. Devadas, *J. Catal.* **1997**, *172*, 475 – 478.

[15] M. Xin, E. Xing, X. Gao, Y. Wang, Y. Ouyang, G. Xu, Y. Luo, X. Shu, *Ind. Eng. Chem. Res.* **2019**, *58*, 6970 – 6981.

[16] C.-Y. Hsieh, Y.-Y. Chen, Y.-C. Lin, *Ind. Eng. Chem. Res.* **2018**, *57*, 7742 – 7751.

[17] K. C. Szeto, Z. R. Jones, N. Merle, C. Rios, A. Gallo, F. Le Quemener, L. Delevoye, R. M. Gauvin, S. L. Scott, M. Taoufik, *ACS Catal.* **2018**, *8*, 7566 – 7577.

[18] a) G. D. Meitzner, E. Iglesia, J. E. Baumgartner, E. S. Huang, *J. Catal.* **1993**, *140*, 209 – 225; b) K. M. Dooley, G. L. Price, V. I. Kanazirev, V. I. Hart, *Catal. Today* **1996**, *31*, 305 – 315; c) N. Rane, A. R. Overweg, V. B. Kazansky, R. A. van Santen, E. J. M.

Hensen, *J. Catal.* **2006**, *239*, 478 – 485; d) V. B. Kazansky, I. R. Subbotina, R. A. van Santen, E. J. M. Hensen, *J. Catal.* **2005**, *233*, 351 – 358; e) E. Mansoor, M. Head-Gordon, A. T. Bell, *ACS Catal.* **2018**, *8*, 6146 – 6162.
[19] L. Meng, X. Zhu, B. Mezari, R. Pestman, W. Wannapakdee, E. J. M. Hensen, *ChemCatChem* **2017**, *9*, 3942 – 3954.
[20] I. Nowak, J. Quartararo, E. G. Derouane, J. C. Védrine, *Appl. Catal. A* **2003**, *251*, 107 – 120.
[21] J. Z. Hu, C. Wan, A. Vjunov, M. Wang, Z. Zhao, M. Y. Hu, D. M. Camaioni, J. A. Lercher, *J. Phys. Chem. C* **2017**, *121*, 12849 – 12854.
[22] a) C. Sun, J. Deng, L. Kong, L. Chen, Z. Shen, Y. Cao, H. Zhang, X. Wang, *IOP Conf. Ser. Mater. Sci. Eng.* **2017**, *275*, 012046; b) N. V. Golubev, E. S. Ignat'eva, V. N. Sigaev, A. Lauria, L. De Trizio, A. Azarbod, A. Paleari, R. Lorenzi, *Phys. Chem. Chem. Phys.* **2015**, *17*, 5141 – 5150.
[23] a) K. Nishi, K.-i. Shimizu, M. Takamatsu, H. Yoshida, A. Satsuma, T. Tanaka, S. Yoshida, T. Hattori, *J. Phys. Chem. B* **1998**, *102*, 10190 – 10195; b) K.-i. Shimizu, M. Takamatsu, K. Nishi, H. Yoshida, A. Satsuma, T. Tanaka, S. Yoshida, T. Hattori, *J. Phys. Chem. B* **1999**, *103*, 1542 – 1549.
[24] a) D. Ma, Y. Shu, C. Zhang, W. Zhang, X. Han, Y. Xu, X. Bao, *J. Mol. Catal. A* **2001**, *168*, 139 – 146; b) B. Zheng, W. Hua, Y. Yue, Z. Gao, *J. Catal.* **2005**, *232*, 143 – 151; c) A. Arnold, S. Steuernagel, M. Hunger, J. Weitkamp, *Microporous Mesoporous Mater.* **2003**, *62*, 97 – 106.
[25] W. Dai, L. Yang, C. Wang, X. Wang, G. Wu, N. Guan, U. Obenaus, M. Hunger, L. Li, *ACS Catal.* **2018**, *8*, 1352 – 1362.
[26] R. Fricke, H. Kosslick, G. Lischke, M. Richter, *Chem. Rev.* **2000**, *100*, 2303 – 2406.
[27] D. J. Parrillo, C. Lee, R. J. Gorte, D. White, W. E. Farneth, *J. Phys. Chem.* **1995**, *99*, 8745 – 8749.
[28] A. Ghorbanpour, J. D. Rimer, L. C. Grabow, *Catal. Commun.* **2014**, *52*, 98 – 102.
[29] A. Ghorbanpour, J. D. Rimer, L. C. Grabow, *ACS Catal.* **2016**, *6*, 2287 – 2298.
[30] A. J. Jones, R. T. Carr, S. I. Zones, E. Iglesia, *J. Catal.* **2014**, *312*, 58 – 68.
[31] C.-M. Wang, R. Y. Brogaard, B. M. Weckhuysen, J. K. Nørskov, F. Studt, *J. Phys. Chem. Lett.* **2014**, *5*, 1516 – 1521.
[32] R. Khare, D. Millar, A. Bhan, *J. Catal.* **2015**, *321*, 23 – 31.
[33] M. Oleksiak, J. D. Rimer, *Rev. Chem. Eng.* **2014**, *30*, 1 – 49.
[34] a) M. D. Oleksiak, K. Muraoka, M. F. Hsieh, M. T. Conato, A. Shimojima, T. Okubo, W. Chaikittisilp, J. D. Rimer, *Angew. Chem. Int. Ed.* **2017**, *56*, 13366 – 13371; *Angew. Chem.* **2017**, *129*, 13551 – 13556; b) R. Gounder, E. Iglesia, *Angew. Chem. Int. Ed.* **2010**, *49*, 808 – 811; *Angew. Chem.* **2010**, *122*, 820 – 823; c) B. C. Knott, C. T. Nimlos, D. J. Robichaud, M. R. Nimlos, S. Kim, R. Gounder, *ACS Catal.* **2018**, *8*, 770 – 784.
[35] J. Towns, T. Cockerill, M. Dahan, I. Foster, K. Gaither, A. Grimshaw, V. Hazlewood, S. Lathrop, D. Lifka, G. D. Peterson, R. Roskies, J. R. Scott, N. Wilkins-Diehr, *Comput. Sci. Eng.* **2014**, *16*, 62 – 74.

Manuscript received: May 17, 2020
Revised manuscript received: August 1, 2020
Accepted manuscript online: August 3, 2020
Version of record online: September 11, 2020

